CSM
Chemistry of Solid Materials
Vol. 1 No. 1 2013

Fabrication and nanostructural characterization of TiO_2 nanorods

M. Riazian
Assistant Professor, Department of Engineering, Tonekabon branch, Islamic Azad University, Tonekabon, Iran
E-mail: m.riazian@tonekaboniau.ac.ir

(Received: July 2013, Accepted: September 2013)

ABSTRACT
TiO_2 nanorods are synthesized by a thermal corrosion. In present work, synthesis of TiO_2 nanorods in anatase, rutile and Ti_8O_{15} phases, by using the sol-gel method and alkaline corrosion are reported. The morphologies and crystal structures of TiO_2 nanorods are characterized by use of field emission scanning electron microscopy, atomic force microscopy and X-ray diffractometer techniques. The obtained results illustrate an aggregated structure at high calcined temperatures with the production of spherical particles. The effects of chemical compositions and calcined temperatures on surface topography and crystallization of phases are studied. Moreover, activation energy of nanoparticles formation is calculated during thermal treatment.

Keywords: Nanostructur, TiO_2 Nanorods, Sol-gel method.

1. INTRODUCTION

TiO_2 is an important material that is used in many industrial applications related to photo-splitting of water [1], photocatalysis [2], photovoltaic devices [3], etc. It is known to have three natural polymorphs, i.e., rutile, anatase, and brookite. The photocatalytic performance of this compound depends on the characteristic of the TiO_2 crystallites, such as the size and surface the area. Therefore, modifications of its physical and chemical properties are of interest to researchers [4-9]. One possible way to modify the properties of TiO_2 crystallites is by adding a second semiconductor into the TiO_2 matrix. Many studies addressing both TiO_2 doping with different metals and the synthesis and characterization of one-dimensional (1D) nanostructures (nanowires, nanotubes, nanorods) have received considerable attention due to unique properties and novel applications of these nanostructures [10-13].
Many methods have been successfully developed for the fabrication of 1D nanostructures, including vapor-solid, vapor-liquid-solid and solution-liquid-solid template-based synthetic approaches and laser ablation [14-19]. However, almost all of these methods either use catalyst materials or physical templates, which unavoidably bring some contamination to the products. Therefore, one has to explore a new approach to synthesize 1D nanomaterials without using preformed templates or catalysts. The sol-gel process is employed quite often for the synthesis of nanosize catalytic mat-erials. The incorporation of an active metal in the sol during the gelation stage allows the metal to have a direct interaction with the support.
In the present work, TiO_2 nanorod is synthesized using a hydrolysis pro-

cedure in simple wet chemical approach with titanium tetra isopropoxide. The obtained results indicated the nanorod properties depend on the preparation procedures and calcination temperature.

2. EXPERIMENTAL

2.1 Reagents and Materials

The preparation method of TiO_2 nanorods have been cited [4]. The composition of the starting solution and the experimental conditions used for the TiO_2 nanorods are listed in Table 1. Fig. 1 illustrates the preparation procedures. The precursors, titanium tetra isopropoxide (TTIP) ($Ti(OPr^i)_4$, Merck ≥98%), 0.1 N nitric acid (Merck≥65%, Ethanol (Merck≥97%) and distilled water are used without further purification.

Table 1. Composition of starting solutions and experimental conditions for TiO_2 nanorods preparation.

Method used	Method step	Precursor	Molar ratio (MR)	Stirring Time (h)	pH
Alkoxide route	1	TTIP	TTIP /EtOH/H_2O =1:0.022/$_{9.5\times10^{-4}}$	24	5

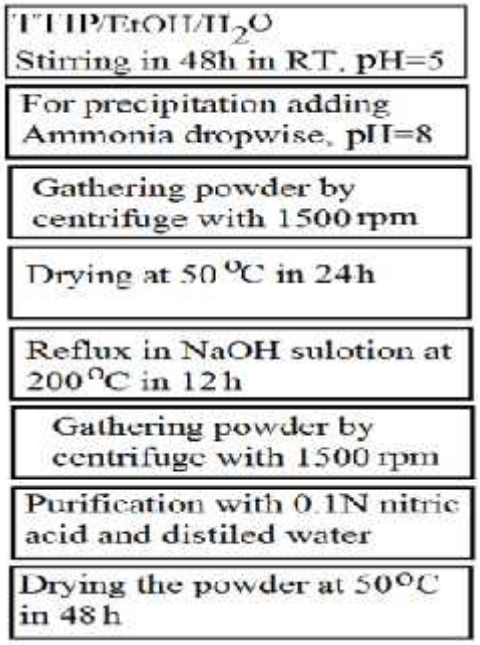

Fig. 1. Schematic flowchart illustrating the steps in the synthesis pathway of TiO_2 nanorods.

The starting point for the synthesis of a targeted system is a solution prepared by mixing the precursors. In detail, according to the molar ratio in Table 1 precursors are chosen (TTIP, deionized water, ethanol). Then, for precipitation, ammonia solution is added dropwise so that pH=8 and is then centrifuged at 1500 rpm to gather the precipitate. The precipitate is heated at 50 ^{0}C for 24 h. For the formation of a rod shape the powders are immersed in 10 N NaOH solution in a teflon balloon at 200 ^{0}C in 6 and 12 h. Once more, the powders are

gathered with a centrifuge and are purified with 0.1 N nitric acid and distilled water to eliminate the Na ions.

2.2 Characterization

XRD patterns measured on a (GBC-MMA 007 (2000)) X-ray diffracto-meter. The diffractograms recorded with ((K_α(Cu), 1.54056Å, 0.02^o step size in which the speed 10^o/min) radia-tion over a 2θ range of 10^o–80^o. Transmission electron microscopy (TEM) (CM10 Philips) was used to investigate the structure and morpho-logy of the nanorods. Field-emission electron microscopy (FE-SEM) (S-4160 Hitachi) was used to investigate the morphology of the nanoparticles. AFM (Easy Scan 2 Flex (Switzerland), silicon tip was used. The measurements made at 20 ^{o}C and relative humidity of 45%. FT-IR measurement was perfor-med on a 1730 Infrared Fourier Tran-sform Spec-trometer (Perkin-Elmer) using the potassium bromide as the background.

3. RESULTS AND DISCUSSION

Crystalline phases of the composite ceramic have been investigated by using XRD technique and the results are shown in Fig. 2. Characteristics of the XRD peaks are summarized in Tables 2. As shown in Fig. 2, different crystalline phases are formed with different calcination treatments. Fig. 2 also shows the amorphous stru-cture of as-prepared and 300 ^{o}C sample due to short range ordering of network [15,17, 20]. Therefore, samples obta-ined at 600 ^{o}C and 900 ^{o}C have a high degree of crystallinity. The grain size has been calculated using Scherrer's equation given by:

$$r = \frac{k^{a}}{2\ cos^{-}} \qquad (1)$$

where β is FWHM observed, shape factor k is assumed to be 0.9 and λ is a wavelength of CuKa radiation (0.154-056 nm).

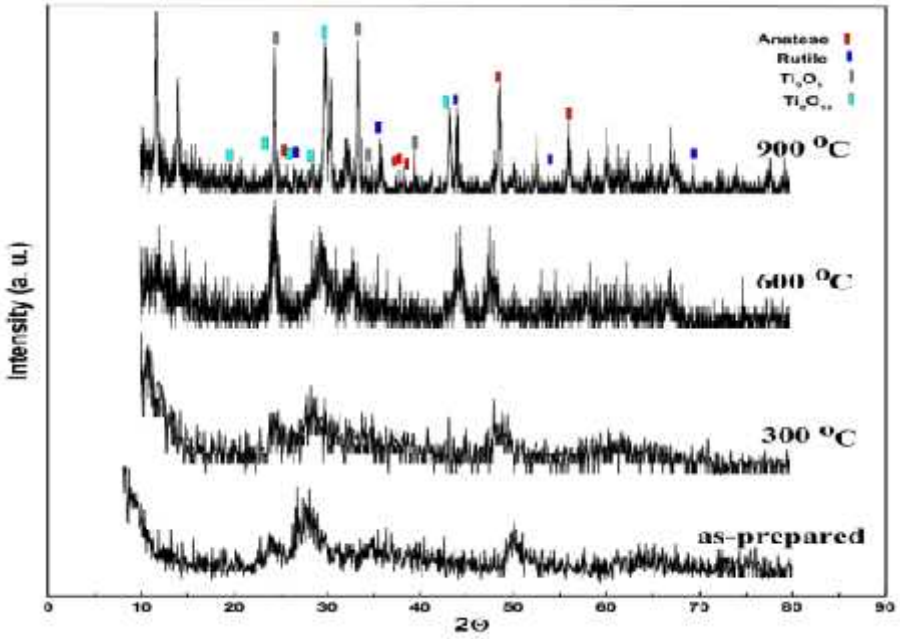

Fig. 2. XRD patterns of TiO_2 nanorod obtained from as-prepared calcined at 300 ^{o}C calcined at 600 ^{o}C and calcined at 900 ^{o}C.

Data in Table 2 shows the influence of calcined temperatures on grain size of different phases. Gradually the size of grains increases when the calcined temperature is increased due to the en-larged chemical bonding.

The average crystallite size has been calculated based on the Scherrer's formula. It can be indicated that the crystallite size of rutile increases rapidly from about 31nm at 600 ^{o}C to 145 nm at 900 ^{o}C, while crystallite size of anatase slowly increases. Phase transformation occurs due to two main effects: surface energy and precursor chemistry. At very small particle dimensions, the surface energy is an important part of total energy and it has been found that surface energy of anatase is lower than those of rutile and brookite [21, 22]. Secondly, crystal structure stability has been explained on the basis of a molecular picture, where nucleation and growth of different polymorphs of TiO_2 are determined by precursor chemistry, which depends on the reactants used [23-25]. Rutile crystals are known to grow much faster than anatase [26]. So, generally, with increasing the calcined temperature, rutile nanocrystals exhibit larger diameters [27]. Anatase nanocrystals have been reported to be more stable at extremely small diameters. However, they have been reported to exist up to 80 nm.

Table 2. The 2θ angle, d-space, Miller indexes, grain size of TiO_2 nanorod.

Crystalline Phase	As-prepared			Calcined at 300 ^{o}C			Calcined at 600 ^{o}C			Calcined at 900 ^{o}C		
	2Θ	d-space(Å)	size(nm)	2Θ	d-space(Å)	size(nm)	2Θ	d-space(Å)	size(nm)	2Θ	d-space(Å)	size(nm)
Anatase Tetragonal a=3.8040 Å c=9.6140 Å	**25.33**	**3.51**	**11**	**25.15**	**3.52**	**34**	**25.60**	**3.46**	**54**	**25.20**	**3.55**	**60**
Rutile Tetragonal a=4.5940 Å c=2.9590 Å	**27.55**	**3.23**	**7**	**27.68**	**3.26**	**18**	**27.56**	**3.23**	**31**	**27.80**	**3.20**	**145**
Ti_2O_3 Hexagonal a=5.1490 Å c=13.6420 Å	**33.2**	**2.69**	**4**	**33.20**	**2.65**	**9**	**33.00**	**2.71**	**13**	**33.35**	**2.69**	**24**
Ti_8O_{15} Hexagonal a=4.8440 Å c=13.2700 Å	**29.10**	**3.06**	**4**	**29.00**	**3.08**	**7**	**29.28**	**3.05**	**12**	**29.8**	**2.99**	**24**

The particle growth kinetics under hydrothermal conditions are determined by coarsening and aggregation–recrystallization processes, allowing control over average nanoparticle size.

In addition, the crystallite size of Ti_2O_3 and Ti_8O_{15} increases rapidly from about 13 and 12 nm at 600 °C to 24 nm at 900 ^{o}C, respectively. This is directly related to the crystallization of nanoparticles.

Then, straight lines of *lnD* against *1/T* (Fig. 3) is plotted according to Scott's equation [28] given below under the condition of homogeneous nanocrystallites growth approximately describing crystal growth during annealing as follows:

$$D=Cexp(-E/RT) \qquad (2)$$

Where *C* is a constant, *E* is activation energy, *R* is gas constant, and T is absolute temperature. The value of *E* is shown in Table 3. It shows that the calcined temperature has a remarkable effect on nanocrystallites growth.

Table 3. The activation energy of nanoparticles formation.

Crystallite phase	**Activation energy** kJ/mol
Anatase	5.78
Rutile	6.15
Ti_2O_3	5.41
Ti_8O_{15}	5.81

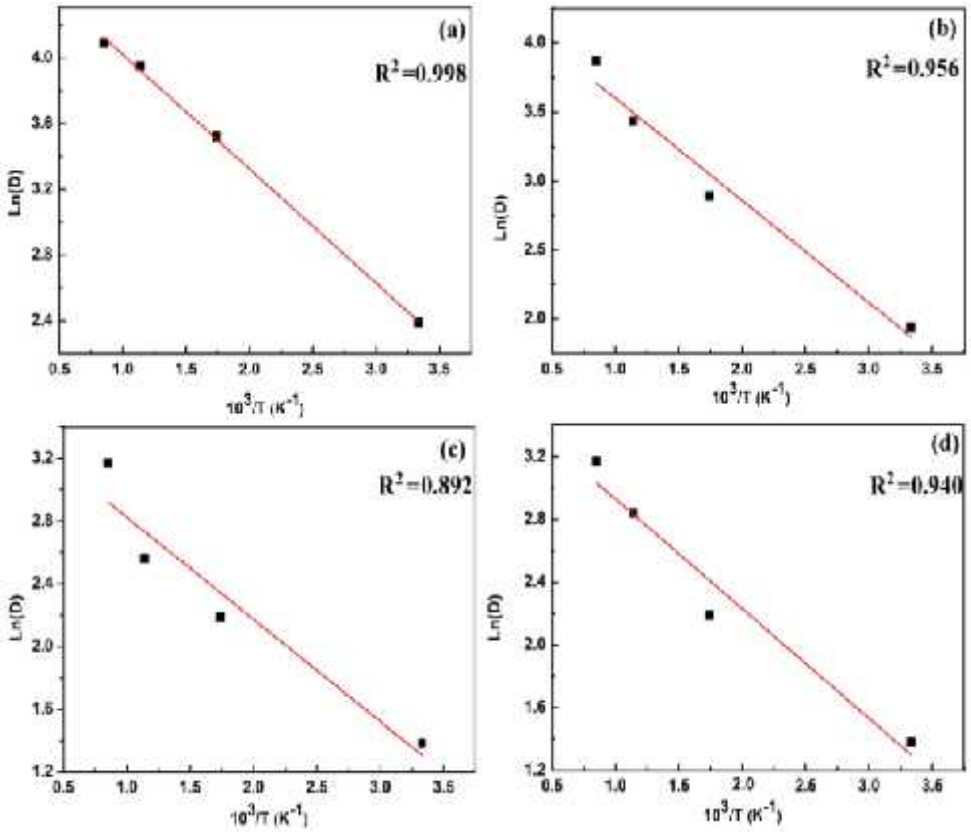

Fig. 3. Plot of LnD as a function of calcination temperature for the (a) anatase (b) rutile (c) Ti_2O_3 (d) Ti_8O_{15}

Lattice strain (ε) of nanocrystallites are determined for dependence of FWHM (Full Width Half Maximum) on diffraction lines observed in 2θ range of 10-80^o on sinθ according to William-son-Hall's equation [29]:

$$cos^{-} = \frac{k^{a}}{L} + 4£\ sin^{-} \qquad (3)$$

where β is FWHM, shape factor k is assumed to be 0.9 similar to Scherrer equation and λ is wavelength of $K_{-}(Cu)$. The plots of βcosθ against 4sinθ for different samples are approximated to be linear. Lattice strain is determined from the slope of this linear relation. Because of lowly-crystallized powder samples, the linearity between βcosθ and 4sinθ is not very good [30]. The plots of βcosθ against 4sinθ for different diffraction lines are illustrated in Fig. 4. For low calcined temperatures, experimental points for diffraction lines are scattered because the peaks are weak and broad so that their

FWHMs are difficult to be measured. It can be seen that lattice strain decreases by increasing the calcined temperature. With increasing the calcined temperature up to 600 ^{o}C, lattice strain decreases from 0.8048 to 0.1019 and with more increasing from 600 ^{o}C to 900 ^{o}C, lattice strain increases from -0.2783 to -0.0991. This implies that with increasing calcined temperature, form of lattice strain varies from external to internal strain.

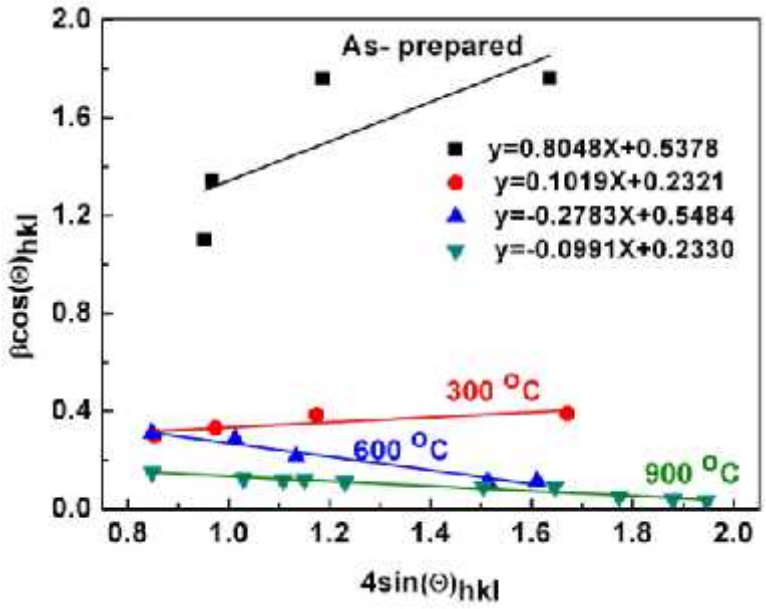

Fig. 4. Plot Relation between βcosθ and 4sinθ (Williamson-Hall plots) with different calcined temperatures.

Fig. 5 shows nanorod structure at 900 ^{o}C. As shown in Fig. 5, the diameter is 43 nm and the length is 400 nm. The FE-SEM images of TiO_2 nanorods is shown in Fig. 6. As-prepared sample has spherical coverage but contains many rods. It seems that nanoparticles are formed in thin rope shape. The particles with spherical coverage with diameter about 560 nm is observed. Fig. 6 shows that the rods are formed at high temperature viz 600 ^{o}C and 900 ^{o}C. Shape of the particles is similar to each other and likely beco-mes rod in general at calcined tempe-ratures of 300, 600 and 900 ^{o}C. It is seen that particles agglomerate when calcined at 300, 600 and 900 ^{o}C. Agglomeration may result from the calcination treatment conditions. How-ever, size distribution of the particles has not been determined.

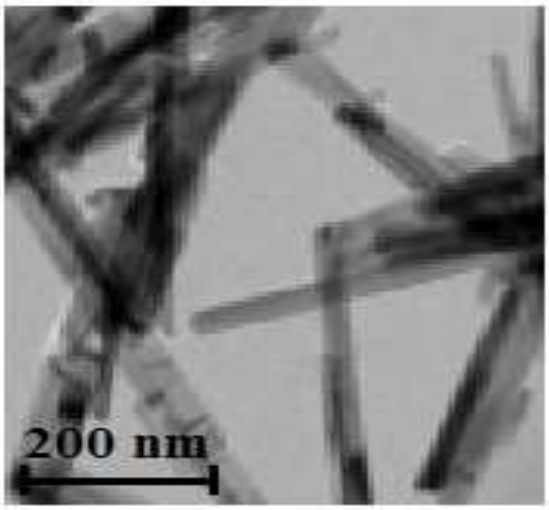

Fig. 5. TEM image of nanorod structure.

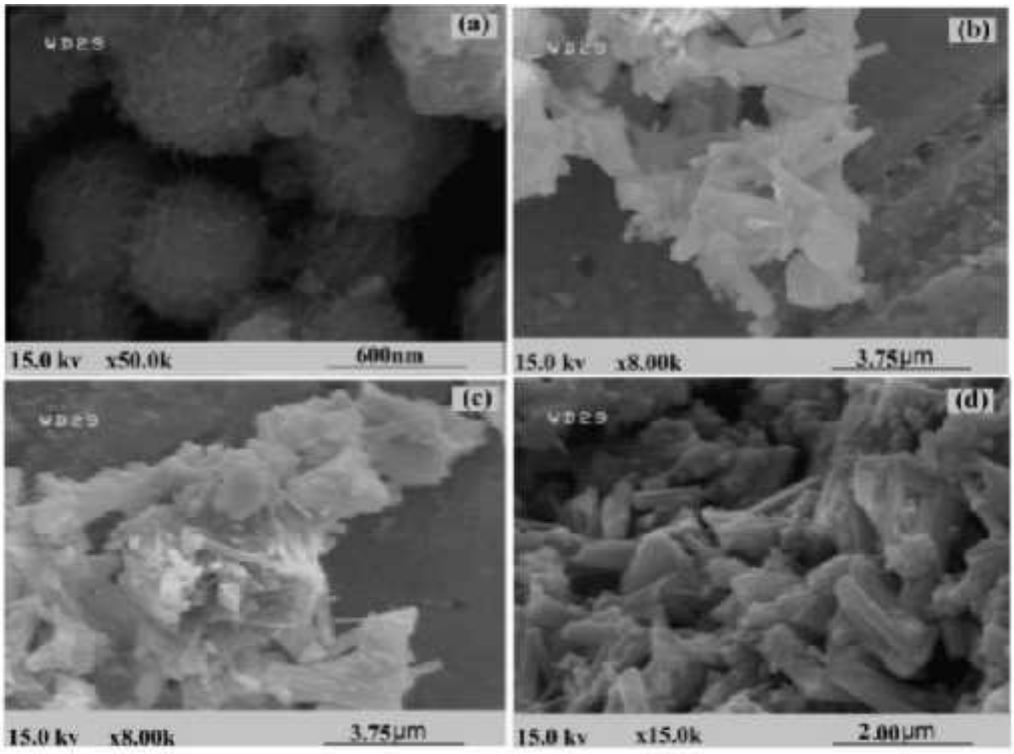

Fig. 6. FE-SEM images of TiO_2 nanorods in different calcined temperatures, (a) as-prepared, (b) 300 ^oC, (c) 600 ^oC and (d) 900 ^oC.

Surface morphology of TiO_2 nanorods is shown in Fig. 7. As shown in this figure, the islands have quite compact shape with length of 2 to 3.5 µm, after the islands are changed into arm-like shapes. The growth reflects continuous presentation of dendritic or irregular pattern while maintaining an arm width of about 6 µm. In fact, two issues affect on the rod structures: (i) Diffusion of adatoms into the matrix at higher concentration and a larger fraction of deposited TiO_2. These adatoms can diffuse off of the first island and condense at the step edge, thereby thickening the structure. (ii) Formation of fractals, where nanoaggregates shapes have been formed. As the linear

size of islands become larger, a higher percentage of TiO_2 makes up fractal regions between the arms. TiO_2 atoms in these regions tend to fill in and do not contribute to further radial growth. Radial growth, on the other hand, is slowed to the extent that islands have not been coalesced and can still be identified as individual entities. The dendritic shapes are due to kinetic limitation existing at room temperature, which can be concluded from their thermal instability [31].

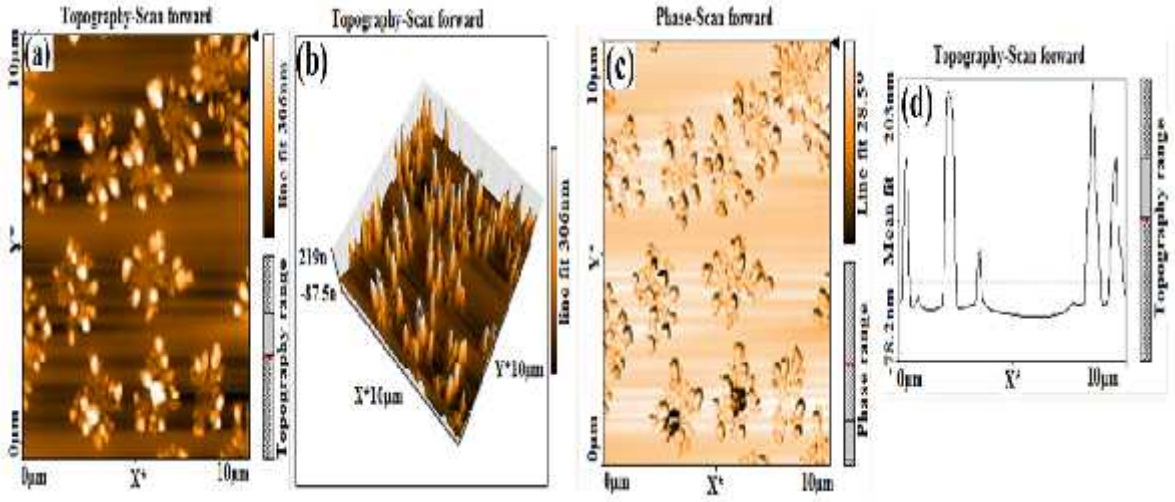

Fig. 7. AFM images of as-prepared TiO_2 nanorods, (a) topography-scan forward, (b) topography-3D scan forward, (c) phase-scan forward and (d) roughness and topography-scan forward.

Surface morphologies are characterized by average thickness of the sheets, intervals between the sheet and the roughness parameters such a S_a, S_m and S_q shown in Table 5. The parameter S_a is the roughness average given by:

$$S_a = \frac{1}{N}\sum_{l=0}^{N-1}\left|Z(x_l)\right| \qquad (4)$$

Moreover, S_m is the mean value given by:

$$S_m = \frac{1}{N}\sum_{l=0}^{N-1} Z(x_l) \qquad (5)$$

and the parameter S_q is the root mean square given by:

$$S_q = \sqrt{\frac{1}{N}\sum_{l=0}^{N-1}(Z(x_l))^2} \qquad (6)$$

Table 5. Roughness parameter of TiO_2 nanorods.

Sample	S_a (nm)	S_q (nm)	S_m (pm)
TiO_2 nanorods in Fig. 7. (a)	34.979	54.599	45.987

The FTIR spectra of TiO_2 nanorods calcined at different temperatures are shown in Fig. 8. In the prepared gel, 3200 cm^{-1} band has to be attributed to hydroxyl groups from water and ethanol occluded in titania pore. Besides, OH bending band of water in gel is observed at 1650 cm^{-1} and low energy interval Ti-O band are found at 1061 and below 1000 cm^{-1}. This band is more significant at 900 ^oC. The IR spectra show characteristic peaks of Ti-O-Ti (495-436 cm^{-1}) [30]. When the composite is calcined at 900 ^oC, high-energy stretching band almost vanishes and 1650 and 3200 cm^{-1} bending vibration band intensity decreases due to vaporization of the liquid.

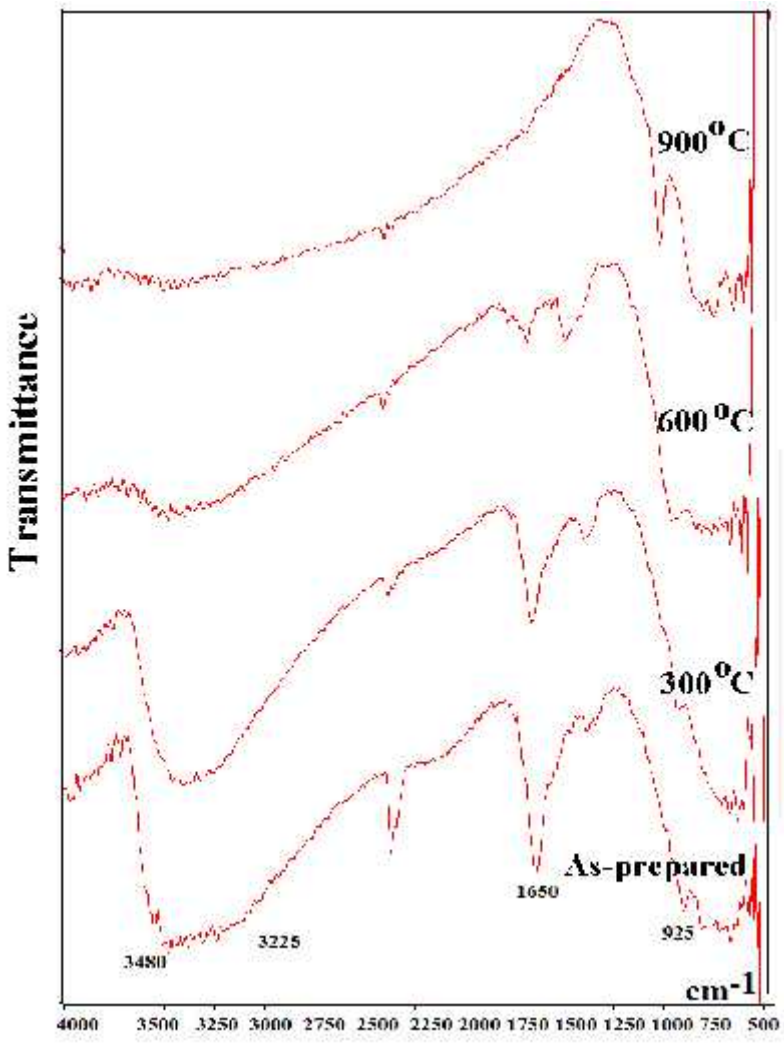

Fig. 8. FTIR spectra of TiO_2 nanorod calcined at different temperatures.

4. CONCLUSION

The homogeneous hydrolysis of metal alkoxide and corrosion with NaOH provides an excellent technique to prepare TiO_2 nanorod materials. Experimental results indicate that homogeneous hydrolysis of titanium tetra isopropoxide via sol-gel route is a promising technique for preparing photosensitive material by uniform nanoparticles. The influence of calcined temperatures can affect structural properties such as size, strain and activation energy. The average crystallite sizes increase with an increase in calcined temperatures.

Acknowledgements

The author thanks Islamic Azad University, Tonekabon branch for financial support of the research project.

REFERENCES

[1] Y. Kim and M. Kang, *Int. J. Photoenergy* 10, 618642 (**2012**).

[2] H. F. Lai, C. C. Chen, J. R. Wu and S. C. Lu, *J. Chin. Chem. Soc.* 59, 89 (**2012**).

[3] A. Loiudice , A. Rizzo , L. D. Marco , M. R. Belviso , G. Caputo , P. D. Cozzoli and G. Gigli, *Phys. Chem.* 21, 3987 (**2012**).

[4] M. Riazian and A. Bahari, *Pramana J. Phys.* 78, 319 (**2012**).

[5] M. Riazian and A. Bahari, *Int. J. Physical Sci.* 6, 3756 (**2011**).

[6] M. Riazian, N. Montazeri and E. Biazar, *Oriental J. Chem*. 27, 903 (**2011**).

[7] M. Riazian and A. Bahari, Int. *J. Nano Dimensions*, 3, 297 (**2013**).

[8] D. N. Gupta, K. R. Sahu, I. Das, A. De and U. De, *Indian J. Phys*. 84, 1413 (**2010**).

[9] M. R.Vaezi, S. K. Shendy and T. J. Ebadzadeh, *Indian J. Phys*. 86, 9 (**2012**).

[10] N. Iguchi, C. Cady, R. Snoeberger, B. Hunter, E. Sproviero, C. Schm-uttenmaer, R. Crabtree, G. Brudvig and V. S. Batista, , *Physical Chemistry of Interfaces and Nanomaterials* VII, Proc. Of SPIE (**2008**) 70340.

[11] Y. Xie, H. Qian, Y. Zhong, H. Guo and Y. Hu, *Int. J. Photoenergy* 10, 682138 (**2012**).

[12] R. Jayasinghe, A. G. Unil Perera and Y. Zhao, *Bull. Ame. Phys. Soc.*, 57, 93 (**2012**).

[13] J. Qiu , F. Zhuge , Xn. Li , X. Gao , X. Gan , L. Li , B. Weng , Z. Shi and Y. Hwae, *J. Mat. Chem*. 22: 3549 (**2012**).

[14] M. A. Pugachevskii, *Phys. Astron.* 38, 328 (**2012**).

[15] H. Wang , Y. Liu , Z. Liu , H. Xu , Y. Deng and H. Shen, Cryst. *Eng. Comm.*, 14, 2278 (**2012**).

[16] E. J. Schwalbach, S. H. Davis, P. W. Voorhees, J. A. Warren and D. Wheeler, *J. Appl. Phys*. 111, 24302 (**2012**).

[17] S. R. Gajjela, C. Yap, M. Grätzel and P. Balaya, *Energy Environ. Sci*., 3, 838 (**2011**).

[18] S. Mitra, A. Mandal, S. Banerjee, A. Datta, S. Bhattacharya, A. Bose and D. Chakravorty, *Indian J. Phys*. 85, 649 (**2011**).

[19] H. Rath, S. Anand, M. Mohapatra, P. Dash, T. Som, U. P. Singh and N. C.Mishra, *Indian J. Phys*. 83, 559 (**2009**).

[20] Prasai, B. Cai, M. K. Underwood, J. P. Lewis and D. A. Drabold, J. *Mater. Sci*., 12, 6439 (**2012**).

[21] Q. Li, et al., *Mater. Sci*. 900, 1828 (**2012**).

[22] H. Zhang and J. Banfield., *J. Mater. Chem.* 8, 2073 (**1998**).

[23] H. Zhang and J. Banfield., *J. Phys. Chem.* B 104, 3481 (**2000**).

[24] P. K. Naicker, P. T. Cummings, H. Zhang and J. F. Banfield., *J. Phys. Chem.* B 109, 15243 (**2005**).

[25] K. Yanagisawa, Y. Yamamoto, Q. Feng and N. Yamasaki., *J. Mater. Res.* 13 825 (**1998**).

[26] K. Yanagisawa and J. Ovenstone., *J. Phys. Chem.* B 103, 7781 (**1999**).

[27] N. Khlomanov et al., *Nanotechnology* 14, 1168 (**2003**).

[28] K. R. Zhu, M. S. Zhang, J. M. Hong and Z. Yin *Mater. Sci. Eng. A* 403, 87 (**2005**).

[29] M. G. Scott Amorphous Metallic Alloys (London: Butterworth) p 151 (**1983**).

[30] A. K. Zak. W. H. Abd Majid, M. E. Abrishami and R. Yousefi, , *Solid State Sci.* 13, 251(**2011**).

[31] M. Inagaki, R. Nonaka, B. Tryba and A. W. Morawski, *Chemosphere*, 64, 437 (**2006**).

[32] J. Ivancoa, T. Haberb, J. R. Krenna, F. P. Netzera, R. Reselb, M. G. Ramseya, *Surf. Sci.* 601, 178 (**2007**).

ساخت و ویژگی‌های نانو میله‌های TiO_2

م. ریاضیان

استادیار گروه شیمی دانشگاه آزاد اسلامی واحد تنکابن، تنکابن، ایران

(تاریخ دریافت: تیر ۱۳۹۲- تاریخ پذیرش: شهریور ۱۳۹۲)

چکیده:

نانو میله‌های TiO_2 توسط خوردگی حرارتی سنتز شده‌اند. در این تحقیق سنتز نانو میله‌های TiO_2 در شکل‌های آناتاز، روتیل و فاز Ti_8O_{15} با استفاده از روش سل ژل و خوردگی قلیایی گزارش شده است. مورفولوژی و ساختارهای کریستالی نانو میله‌های TiO_2 با تکنیک های میکروسکوب الکترونی روبشی نشر میدانی، میکروسکوب نیروی اتمی و پراش اشعه ایکس مشخصه یابی گردید. نتایج بدست آمده یک ساختار تجمع یافته در دما های کلسینه بالا با تولید ذرات کروی را نشان می‌دهند. اثرات ترکیب اجزای شیمیایی و دماهای کلسینه روی مورفولوژی سطح و بلوری شدن فازها مطالعه شده است. علاوه بر این انرژی فعالسازی تشکیل نانو ذرات به هنگام اعمال گرمایی محاسبه شده است.

m.riazian@tonekaboniau.ac.ir